condensed matter

MDPI

Article

Impact of Lattice Vibrations on the Dynamics of a Spinor Atom-Optics Kicked Rotor †

Caspar Groiseau [1], Alexander Wagner [2], Gil S. Summy [3] and Sandro Wimberger [2,4,5,*]

1 Dodd-Walls Centre for Photonic and Quantum Technologies, Department of Physics, University of Auckland, 92019 Auckland, New Zealand; cgro288@aucklanduni.ac.nz
2 Institute for Theoretical Physics, Heidelberg University, Philosophenweg 12, 69120 Heidelberg, Germany; alexander.l.wagner@gmail.com
3 Department of Physics, Oklahoma State University, Stillwater, OK 74078-3072, USA; gil.summy@okstate.edu
4 Dipartimento di Scienze Matematiche, Fisiche e Informatiche, Università di Parma, Campus Universitario, Parco Area delle Scienze n. 7/a, I-43124 Parma, Italy
5 Italian Institute for Nuclear Physics (INFN), Sezione di Milano Bicocca, Gruppo Collegato di Parma, 43124 Parma, Italy
* Correspondence: sandromarcel.wimberger@unipr.it
† SuperFluctuations 2018: Fluctuations and Highly Non Linear Phenomena in Superfluids and Superconductors, San Benedetto del Tronto, Italy, 5–7 September 2018.

Received: 27 December 2018; Accepted: 8 January 2019; Published: 14 January 2019

Abstract: We investigate the effect of amplitude and phase noise on the dynamics of a discrete-time quantum walk and its related evolution. Our findings underline the robustness of the motion with respect to these noise sources, and can explain the stability of quantum walks that has recently been observed experimentally. This opens the road to measure topological properties of an atom-optics double kicked rotor with an additional internal spin degree of freedom.

Keywords: Bose–Einstein condensates; ultracold atoms; quantum walks; topological phases; dynamical phases

1. Introduction

Following its theoretical proposal in 1992 [1], the atom-optics kicked rotor (AOKR) has proven to be a reliable and useful work horse for studying the dynamical evolution of driven low-dimensional dynamical quantum systems [2–4] for more than twenty years.

Its success has translated into many different fields of research, from Anderson and dynamical localisation [3,5–8] to ballistic quantum resonant motion [9–11]. Many AOKR experiments tested the effect of artificial or natural noise and decoherence [4,5,12–15], and the stability with respect to parameter changes [16–18]. Currently, platforms based on Bose–Einstein condensates offer unprecedented control over the initial conditions in phase space [19–21], which are used to produce directed motion [21–26] and to study dynamical tunnelling [27,28], for instance.

This exceptional control and dynamical stability has recently led to the realisation of discrete-time quantum walks [29]. Moreover, there are numerous proposals to investigate the effects of topological invariants based on extended versions of an AOKR [30–35]. The latter two applications make it necessary to control not only the momentum of the atomic centre of mass degree of freedom, but to include additional degrees of freedom, typically two internal electronic states [36–38] which become entangled with momentum during the temporal evolution. Hence, it is expected that topological properties built on such an effective spin–orbit coupling [39] can be tested with such platforms.

In this paper, we test the stability of the spinor AOKR with respect to noise sources, as it realises (i) the discrete-time quantum walk and (ii) a double kicked rotor system for studying topological phases. We essentially investigate amplitude and phase fluctuations of the standing wave kicking the atoms. Both effects are present in state-of-the-art experiments, and possibly lead to a degradation of the experimental signal. While the original quantum resonant motion proved to be rather robust with respect to amplitude noise [4,40], phase noise is a more serious problem since it destroys the resonant condition on which this regime is based. Phase shifts map via a gauge transform into shifts of the atoms' quasimomenta. Since a Bose condensate cannot be cooled to zero temperature, a residual finite distribution of quasimomenta is present in all experiments, in the best case of a width down to $\sim 1\%$ of the Brillouin zone [20,29]. Therefore, the stability of an actual experiment with respect to lattice phase shifts, either random or effectively induced by the finite quasimomentum distribution, is very relevant to predict the parameter windows within which the proposals of quantum walks and topological phases can be observed.

The paper is organised as follows: Section 2 is devoted to testing the robustness of a discrete-time quantum walk realised by an AOKR with an additional spin degree of freedom. Amplitude and phase noise are studied for perfect quantum resonant conditions. Section 3 tests whether the proposal by Zhou and Gong from Ref. [35] survives realistic amplitude fluctuations and quasimomentum distributions. Our predictions underline the stability of the AOKR motion with respect to weak noise as well as the cross-over to the classical regime of stronger noise where quantum interference is dynamically degraded.

2. Discrete-Time Quantum Walk in Momentum Space

2.1. Quantum Walk Evolution

The AOKR is defined by the following dimensionless Hamiltonian:

$$\hat{H} = \frac{\hat{p}^2}{2} + k\cos(\hat{x}) \sum_{j=1}^{T} \delta(t - j\tau), \tag{1}$$

where p is the momentum, x the position, k the kick strength and τ the period of the kicks. This Hamiltonian is spatially periodic, and therefore only couples momentum states that differ by a multiple of unity (or in experimental units of two photon recoils). Due to Bloch's theorem, we can then separate the momentum into an integer part n and a conserved non-integer part β called quasimomentum

$$p = n + \beta\,. \tag{2}$$

The one-cycle Floquet operator [4] which describes the evolution is given by

$$\hat{\mathcal{U}}_{\beta,k} \;=\; e^{-i\tau(\hat{n}+\beta)^2/2}\, e^{-ik\cos\hat{\theta}}\,, \tag{3}$$

where $\hat{n} = -i\frac{\mathrm{d}}{\mathrm{d}\theta}$ is the (angular) momentum operator with periodic boundary conditions and $\theta = x \bmod (2\pi)$. It is composed of a kick part

$$\hat{K} = e^{-ik\cos\hat{\theta}} \tag{4}$$

and a free evolution part

$$\hat{F} = e^{-i\tau\frac{(\hat{n}+\beta)^2}{2}}\,. \tag{5}$$

The kick period τ and the quasimomentum β can be chosen in such a way that the free evolution part is equal to unity—a regime which defines the principal quantum resonances [4,41]. At these quantum resonances, the momentum distribution normally evolves symmetrically around its initial integer momentum and displays ballistic expansion characterised by a standard deviation which is proportional to the number of kicks (i.e., to time). One can break this symmetry by using a ratchet effect, whereby the initial state breaks the time-reversal symmetry and where the motional direction depends on the sign of the kick strength—see Refs. [4,22,23] for the original idea and our proposal of momentum-state quantum walks [29,38] for details. By tuning the standing-wave laser between two ground-state internal levels of the atoms such that one is negatively and one positively detuned, we can achieve different signs in k, as first proposed in [38]. Then, the single-state kick operator in (4) effectively becomes

$$\hat{K}_{\text{shift}} = \begin{pmatrix} e^{-ik\cos\hat{\theta}} & 0 \\ 0 & e^{ik\cos\hat{\theta}} \end{pmatrix} . \tag{6}$$

Before each of these kicks, we mix both internal levels $|\downarrow\rangle$ and $|\uparrow\rangle$ by applying a 50:50 beam splitter matrix, realising the coin toss of the discrete-time quantum walk:

$$\hat{M}_{\text{coin}} = \hat{M}(\pi/2, -\pi/2) = \frac{1}{\sqrt{2}} \begin{pmatrix} 1 & i \\ i & 1 \end{pmatrix} . \tag{7}$$

This can be generalised to an arbitrary spin rotation given by the two-parameter unitary matrix

$$\hat{M}(\alpha, \chi) = \begin{pmatrix} \cos\frac{\alpha}{2} & e^{-i\chi}\sin\frac{\alpha}{2} \\ -e^{i\chi}\sin\frac{\alpha}{2} & \cos\frac{\alpha}{2} \end{pmatrix} = \exp\left(-i\frac{\alpha}{2}\left[\sin(\chi)\,\sigma_x - \cos(\chi)\,\sigma_y\right]\right) , \tag{8}$$

which will become useful later on in Section 3.1. After the application of a sequence of $\hat{M}_{\text{coin}}\hat{K}_{\text{shift}}$ to appropriately chosen initial states in both degrees of freedom [29,38], the total momentum distribution is computed from the sum of the momentum distributions of both ground-state contributions

$$P(n;T) = P_1(n;T) + P_2(n;T) . \tag{9}$$

$P(n;T)$ is the main observable in the experiment based on a kicked Bose–Einstein condensate [29].

In most of what will be considered here, we assume perfect quantum resonance conditions (e.g., $\tau = 4\pi$ and $\beta = 0$ in Equation (5)). However, Section 3.1 also addresses the degradation of the ideal quantum-walk evolution induced by a finite distribution of quasimomenta around the resonant value. The latter is the experimental situation in which the Bose condensate cannot be prepared exactly at zero temperature, but will always have a finite width of a few percent in the Brillouin zone (which has a size of exactly 1 in our units). The phase fluctuations of the periodic potential considered in the next Section 2.2 have the same effect as changing quasimomentum. Hence, the following results are valuable for realistic predictions of the experiment.

2.2. Lattice Vibrations

During the experiment the standing-wave laser may contain intensity and phase fluctuations. Moreover, each atom experiences a different kick strength k_j depending on its exact spatial position with respect to the beam waist. Therefore, in order to model the experimental fluctuations, we now consider an AOKR system in which the optical lattice kicking the atoms is subject to random changes of its intensity and phase. This changes the typical AOKR Hamiltonian of Equation (1) to

$$\hat{H} = \frac{\hat{p}^2}{2} + \sum_j k_j \cos(\hat{\theta} + \phi_j)\delta(t - j\tau) , \tag{10}$$

where k_j and ϕ_j are random variables. It is straightforward to see that these two variables directly affect the step operator of the quantum walk such that

$$\hat{K}_{\mathrm{fl}} = \begin{pmatrix} e^{-ik_j\cos(\hat{\theta}+\phi_j)} & 0 \\ 0 & e^{ik_j\cos(\hat{\theta}+\phi_j)} \end{pmatrix}. \tag{11}$$

For an AOKR with two internal degrees of freedom, the kicking potential induces a relative light shift, acting as an additional dynamical phase, which must be compensated in order to implement the ideal evolution described by the Hamiltonian (1) [42]. The compensation is done by the coin matrix rotating the internal degree of freedom—see [29,42] for details. The fluctuations in k_j imply that the light-shift phase differs from kick to kick. At the jth step of the walk, it will be

$$\Phi_j = 2k_j\,. \tag{12}$$

Below, we compare results from this optimal compensation and results from the standard compensation of $2k \equiv 2k_0$ [42]. The latter means that the two levels experience an effective light-shift phase equal to the difference of the ideal and the fluctuating kick strength:

$$\Phi'_j = 2(k_j - k_0)\,. \tag{13}$$

If we integrate this latter phase into the coin (7), we can simulate the non-perfect phase compensation in the presence of amplitude noise by the following coin matrix:

$$\hat{M}_{\mathrm{np}} = \frac{1}{\sqrt{2}} \begin{pmatrix} e^{-i\frac{\Phi'_j}{2}} & ie^{i\frac{\Phi'_j}{2}} \\ ie^{-i\frac{\Phi'_j}{2}} & e^{i\frac{\Phi'_j}{2}} \end{pmatrix}. \tag{14}$$

Since random fluctuations are in principle unknown, they cannot be compensated in a real experiment. Hence, a non-optimal compensation with just a phase $2k_0$ without the fluctuating part is much more realistic than (12), and the difference between the two is given by (13).

2.3. Numerical Simulations: Quantum-to-Classical Transitions

The simulations for the lattice vibrations were based on the quantum Floquet map of the kicked-rotor evolution [43], where the free evolution and the kick factorise in the Raman–Nath approximation because the kick is δ-like in time. Free evolution and kick were evaluated in position and momentum space, respectively. We switched back and forth between these two with a standard optimised fast Fourier transform [44]. We averaged the final momentum distribution over 10^4 realisations of the noisy trajectories, corresponding to an average over a similar number of single atoms in the Bose–Einstein condensate [29].

For each walk step j of each realisation, the kick strength from the previous kick was shifted by an amount δk_j randomly drawn from a Gaussian with FWHM Δ_k so that $k_j = k_{j-1} + \delta k_j$ and, starting with $k_0 = 1.45$, a value used in the experiment [29]. Simultaneously, the kick potential was shifted by a phase ϕ_j randomly drawn from a uniform distribution within the interval $\Delta_\phi \times [-\pi;\pi]$. A similar procedure was used in [45] to model the AOKR dynamics without the extra internal degree of freedom.

As with all quantum walks, we expected to see a transition from the quantum regime, dominated by interference effects, to a classical regime characterised by a unimodal classical probability distribution (e.g., a Gaussian or other stable distributions as in [45]) as we introduced decoherence. The transition happened with a constant amount of noise gradually over time, or at constant time for an increasing amount of noise.

For small lattice variations of up to ca. $\Delta_k = 0.1k_0$ or $\Delta_\phi = 0.06$, the quantum walk remained quite stable, see Figure 1. There we also see that the broader the distributions of k_j and ϕ_j the more the walk lost its "quantum" nature and reverted to a classical random walk. For fairly large values of noise, around $\Delta_k = 0.5k_0$ or $\Delta_\phi = 0.3$, and for the chosen number of walk steps $T = 15$, we reached the classical limit (being similar to a Gaussian). This transition happened faster if both noise sources were present simultaneously, as can be seen in Figure 1c,d.

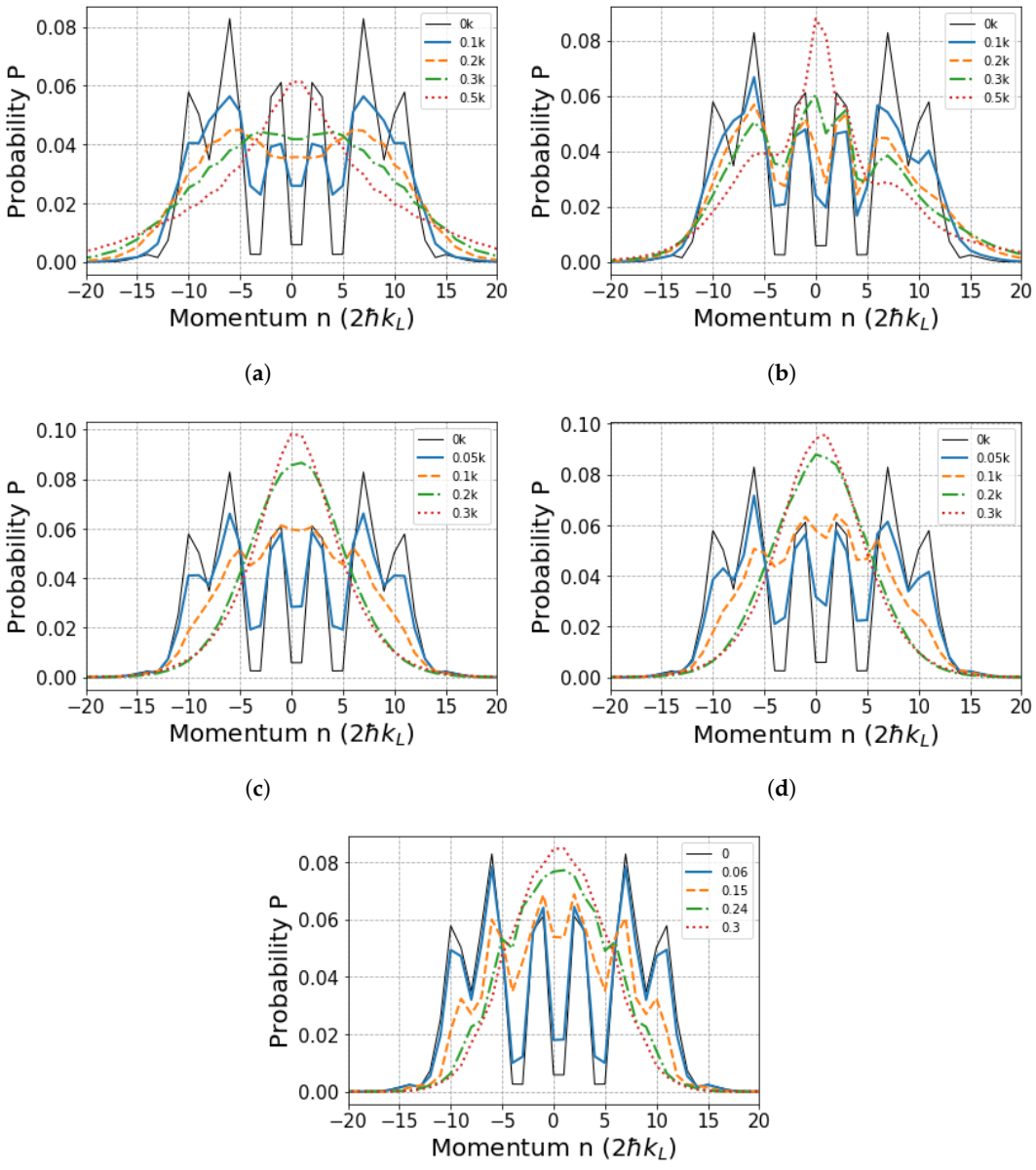

Figure 1. Momentum distributions of quantum walks with kick strength $k \equiv k_0 = 1.45$ after a series of $T = 15$ steps for different noise strengths Δ_k as given in the corresponding legends. Amplitude noise only: (**a**,**b**). Amplitude and phase noise: (**c**,**d**), with equal noise strength $\Delta_\phi = \Delta_k$. Only phase noise in (**e**) with values of Δ_ϕ as given in the legend. The light-shift phase was compensated perfectly in (a,c) and only according to Equation (13) in (b,d). In (e), the compensation was assumed to be perfect since k was constant.

The two different ways of compensating the effective light shift phase described in Section 2.2 led to visible differences in the momentum distribution. If the compensation is not perfect, one expects an asymmetric evolution of the quantum walk. This can be used experimentally to calibrate the

compensation [29]. Note the difference between the cases of amplitude noise in Figure 1a with perfect compensation and Figure 1b with imperfect compensation. However, once phase noise was added there was little difference between cases with (Figure 1c) and without perfect compensation (Figure 1d), as the phase noise tended to have a dominating effect. Hence, adding a small amount of phase noise can help to compensate for the dynamical phase induced by the random light shift (13). This might turn out to be useful for future experiments.

The way the two different noises in amplitude and phase dynamically altered the momentum distributions was slightly different. In Figure 1a we see that amplitude fluctuations led at first, for lower Δ_k, to a decline in the centre of the distribution. The walk continued to spread in a ballistic manner and the bimodal character of the distribution remained conserved for quite a while until the distribution transformed into a function with broad power-law-like tails. The phase fluctuations (see Figure 1e), on the other hand, led to quantum walks which quickly coalesced towards the momentum origin. The distribution in the limit of large Δ_ϕ in that case was Gaussian. A good overview of this dynamical behaviour is provided in Figure 2. Here one can also see that a similar difference between the two noise sources in the quantum-to-classical transition was observed in the time domain.

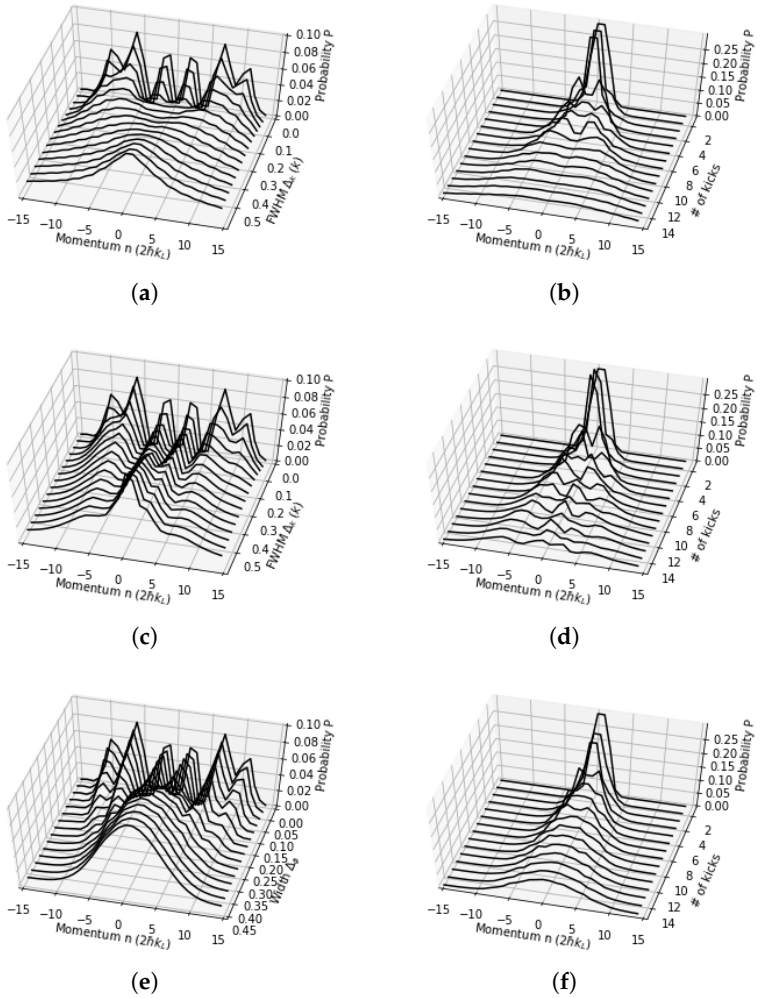

Figure 2. Numerical simulations of the quantum walk with amplitude and phase noise to observe the quantum-to-classical transition. Amplitude noise with (**a**,**b**) and without perfect light-shift compensation (**c**,**d**). Phase noise in (**e**,**f**). (**a**,**c**,**e**) for $T = 15$ as a function of the respective noise strength. (**b**,**d**,**f**) as a function of the number of walk steps for $\Delta_k = 0.3k_0$ in (b,d) and $\Delta_\phi = 0.3$ in (f). Note the similarity of the transitions in the time and noise-strength domain and the disparity of the limiting distributions for both noise effects. Momentum n is given in the experimental units of two photon recoils $2\hbar k_L$, with k_L being the wave vector of the kicking beam.

3. Double Kicked Rotor Evolution

This section deals with an extension of the AOKR to a double sequence of kicks. The double kicked rotor (DKR) is also a periodic system, only with a mapping period of two kicks. A DKR with an additional spin-1/2 degree of freedom allows topological phases with arbitrarily large winding numbers to appear, as was realised and described by Zhou and Gong in Ref. [35]. The experimental realisation of such a system would open the door to experimental explorations of the rich field of topological phases in periodically driven Floquet systems [30,31,34,46–48].

In the following, we rely on the presentation given in [35], only briefly reviewing its results here. Our main concern was to test the robustness of the predicted observable in [35] with respect to typical experimental issues, such as a finite distribution of quasimomenta (making the motion deviate from exact quantum resonance conditions) and amplitude noise in the two kicking lattices of the DKR.

3.1. Proposal

The DKR with internal spin degree of freedom is governed by the following Hamiltonian [35]

$$\hat{H}_{\mathrm{DK}} = \frac{\hat{p}^2 \otimes \mathbb{1}}{2} + k_1 \cos\left(\hat{\theta}\right) \otimes 2\hat{S}_x \cdot \sum_{n=0}^{\infty} \delta(t - 2n\tau) + k_2 \sin\left(\hat{\theta}\right) \otimes 2\hat{S}_y \cdot \sum_{n=0}^{\infty} \delta(t - (2n+1)\tau)\,, \tag{15}$$

where we include both degrees of freedom for brevity. The atoms' center-of-mass degree of freedom is characterized by the operators $\hat{p}$ and $\hat{\theta}$. The internal degree of freedom is represented by the identity operator during the free evolution part and the spin rotations $\hat{S}_i$ in the two kicks (with $i = x, y, z$ in the internal spin-1/2 degree of freedom).

Here we treat the quantum resonant case ($\beta = 0$ at $\tau = 4\pi$) exclusively, meaning that the free evolution terms, Equation (5), are equal to unity. In its two chiral symmetric time frames, this gapped Hamiltonian [35] is characterised by its topological invariant, the winding number [35]. To experimentally measure this invariant, Ref. [35] suggests computing the mean chiral displacement (MCD):

$$C_l(t) = \langle \psi_{in} | \, \hat{U}_l^{-t} \, (\hat{n} \otimes -\sigma_z) \, \hat{U}_l^{t} \, | \psi_{in} \rangle \ . \tag{16}$$

This observable is reminiscent of the fidelity signal measured, for instance, in Refs. [16–18], and of the time-reversed quantum walk recently realised [29]. The only difference is the additional $-\sigma_z$ operator in Equation (16), which simply implies that in order to calculate the MCD we subtract the momentum probability distribution for $|\uparrow\rangle$ from the one for $|\downarrow\rangle$. Here the index l denotes the choice of one out of two chiral symmetric Floquet operators

$$\hat{U}_1 = e^{-\frac{i}{2}k_1 \cos(\hat{\theta})\sigma_x} e^{-ik_2 \sin(\hat{\theta})\sigma_y} e^{-\frac{i}{2}k_1 \cos(\hat{\theta})\sigma_x}, \tag{17}$$

$$\hat{U}_2 = e^{-\frac{i}{2}k_2 \sin(\hat{\theta})\sigma_y} e^{-ik_1 \cos(\hat{\theta})\sigma_x} e^{-\frac{i}{2}k_2 \sin(\hat{\theta})\sigma_y}\,. \tag{18}$$

As discussed in Ref. [35], the average MCD converges towards the winding number

$$\overline{C}_l(t) = \frac{1}{t}\sum_{t'=1}^{t} C_l(t') = \frac{\nu_l}{2} - \frac{1}{t}\sum_{t'=1}^{t} \int_{-\pi}^{\pi} \frac{d\theta}{2\pi} \frac{\cos\left(E(\theta)t\right)}{2} \left(\vec{n}_l \times \partial_\theta \vec{n}_l\right)_3 \quad \overset{t\gg 1}{\longrightarrow} \quad \frac{\nu_l}{2}\,. \tag{19}$$

This holds because with growing t the integrand in the second term in the middle of Equation (19) will oscillate faster and faster. Consequently, we will be integrating over full periods and the integral will vanish. We verified numerically that the convergence starts to become very good for about $t = 10$ steps. However, already by $t = 5$ steps there may be sufficient convergence to see the signal.

To experimentally realise the chiral symmetric Floquet operators with the setup reported in Ref. [29], a decomposition containing only σ_z rotations is needed, and already given in Ref. [35]. Such a

decomposition of the Floquet operators (17) and (18) can be achieved at the additional cost of more rotations applied to the internal state, see Equation (8):

$$\begin{aligned}\hat{U}_1 &= \hat{M}\left(-\frac{\pi}{2},0\right)\ \hat{T}_1\ \hat{M}\left(\frac{\pi}{2},0\right)\ \hat{M}\left(-\frac{\pi}{2},\frac{\pi}{2}\right)\ \hat{T}_2\ \hat{M}\left(\frac{\pi}{2},\frac{\pi}{2}\right)\ \hat{M}\left(-\frac{\pi}{2},0\right)\ \hat{T}_1\ \hat{M}\left(\frac{\pi}{2},0\right)\\ &= \exp\left(i\frac{\pi}{4}\sigma_y\right)\hat{T}_1\exp\left(-i\frac{\pi}{4}\sigma_y\right)\exp\left(i\frac{\pi}{4}\sigma_x\right)\hat{T}_2\exp\left(-i\frac{\pi}{4}\sigma_x\right)\exp\left(i\frac{\pi}{4}\sigma_y\right)\hat{T}_1\exp\left(-i\frac{\pi}{4}\sigma_y\right)\ ,\end{aligned} \tag{20}$$

where

$$\hat{T}_1 = e^{-\frac{i}{2}k_1\cos(\hat{\theta})\sigma_z}, \tag{21}$$

$$\hat{T}_2 = e^{-ik_2\sin(\hat{\theta})\sigma_z}\,. \tag{22}$$

The operator $\hat{U}_2$ can be rewritten in an analogous manner. Through the application of rotations in spin-space, as defined by $\hat{M}(\alpha,\chi)$, we can transform the kick operators $\hat{T}_1$ and $\hat{T}_2$. This allows us to realise the kicks dependent on σ_x and σ_y, by using only kicks dependent on σ_z, as present in the original problem (see Equation (6) in Section 2.1).

3.2. Stability with Respect to Noise

In this section, we check the convergence of the MCD (19) by numerically simulating the DKR for $k_1 = \frac{\pi}{2}$, while varying k_2 in the interval $\left[\frac{\pi}{2}, \frac{5\pi}{2}\right]$. For every choice of k_2, we compute the average MCD and compare it to the step-like structure of half the corresponding winding number (see Equation (19)).

In Figure 3, we examine how perturbations due to experimental imperfections affect the convergence of the average MCD. Since the atoms in the Bose–Einstein condensate exhibit an approximate Gaussian distribution around the resonant quasimomentum $\beta = 0$ [4,18,28,29], we draw a random β from this distribution for every numerical realisation (applies to Figure 3b–d). Moreover, we also consider kick-to-kick amplitude fluctuations in the kicking potential. Before applying a kick in the numerical simulation, we draw a random kicking strength k_1 or k_2 from the corresponding Gaussian distribution and apply the non-perfect light-shift phase discussed previously in Equation (13).

As in Section 2.2, the dominant perturbative effect is now the quasimomentum distribution seen in Figure 3b, since it affects the central resonance condition of the DKR. The kick-to-kick amplitude fluctuations play a subordinate role. It even seems that the light-shift phase partially compensated for the perturbative effect of the quasimomentum distribution. This phenomenon can be seen in Figure 3d for $\overline{C}_1$; it was similar to what was observed in Figure 1d, where the phase shift and the non-perfect light shift tended to compensate for the pertubative effect as well. On the other hand, the convergence of $\overline{C}_2$ was already substantially degraded for the large perturbations depicted in Figure 3d.

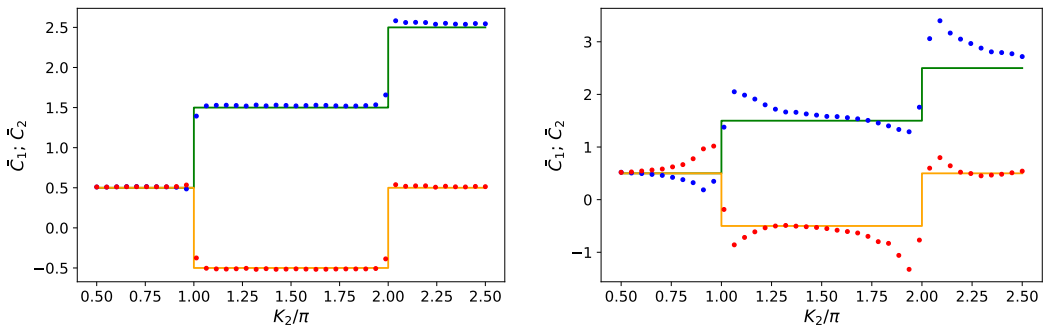

(**a**) Ideal behaviour: no noise (**b**) $\beta_{FWHM} = 1\%$

Figure 3. *Cont.*

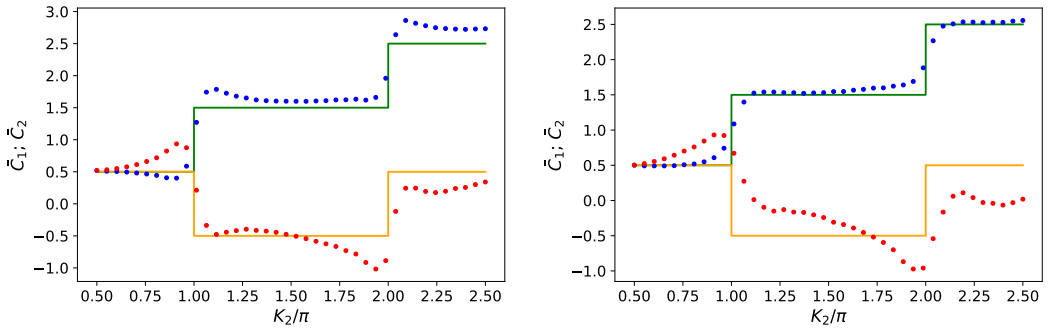

(**c**) $\beta_{FWHM} = 1\%$ and $k_{FWHM} = 15\% \cdot k$ (**d**) $\beta_{FWHM} = 3\%$ and $k_{FWHM} = 30\% \cdot k$

Figure 3. Behaviour of the averaged (over 20 steps) mean chiral displacement $\overline{C}_1(t)$ for the time evolution under $\hat{U}_1$ (in blue) and $\overline{C}_2(t)$ for the time evolution under $\hat{U}_2$ (in red). To check the convergence of $\overline{C}_1(t)$ towards $\frac{\nu_1}{2}$ and $\overline{C}_2(t)$ towards $\frac{\nu_2}{2}$ as stated in Equation (19), $\frac{\nu_1}{2}$ (green) and $\frac{\nu_2}{2}$ (yellow) are plotted as well. The parameter $k_1 = \frac{\pi}{2}$ is kept constant as k_2 is varied. The four panels show the effect of different types of perturbation. All data sets represent averages taken over 1000 realisations (each of which with a fixed initial quasimonentum).

4. Conclusions

We checked the stability of two versions of the AOKR: (i) for a recently realised quantum walk and (ii) for a recent proposal to observe topological phases. Both systems were robust with respect to realistic fluctuations in either amplitude or phase of the kicking lattice. Since the lattice phase corresponds to a shift in the atoms' quasimomentum, the robustness extends to typical initial distributions of quasimomenta present in an AOKR implementation with a Bose–Einstein condensate. Our results explain the good experimental signal of the quantum walks observed in [29], but also give limits for the crossover to the classical regime of such walks. Moreover, the topological properties of a double kicked spinor system as predicted in Ref. [35] turn out to be very stable as well. This should allow for testing of those properties in ongoing experiments.

Author Contributions: Project design: G.S.S. and S.W.; Supervision: S.W.; Data production and visualization: C.G. and A.W.; All authors contributed to the writing of the manuscript.

Funding: A.W. acknowledges funding from the Studienstiftung des deutschen Volkes, in particular a grant for visiting Parma University.

Acknowledgments: S.W. is very grateful to the organisers of the conference *SuperFluctuations 2018* for his invitation.

Conflicts of Interest: The authors declare no conflict of interest.

References

1. Graham, R.; Schlautmann, M.; Zoller, P. Dynamical localization of atomic-beam deflection by a modulated standing light wave. *Phys. Rev. A* **1992**, *45*, R19–R22. [CrossRef] [PubMed]
2. Raizen, M.G. Quantum Chaos with Cold Atoms. *Adv. At. Mol. Opt. Phys.* **1999**, *41*, 43–81. [CrossRef]
3. Bharucha, C.F.; Robinson, J.C.; Moore, F.L.; Sundaram, B.; Niu, Q.; Raizen, M.G. Dynamical localization of ultracold sodium atoms. *Phys. Rev. E* **1999**, *60*, 3881–3895. [CrossRef]
4. Sadgrove, M.; Wimberger, S. A pseudo-classical method for the atom-optics kicked rotor: From theory to experiment and back. *Adv. At. Mol. Opt. Phys.* **2011**, *60*, 315–369.
5. Klappauf, B.G.; Oskay, W.H.; Steck, D.A.; Raizen, M.G. Observation of Noise and Dissipation Effects on Dynamical Localization. *Phys. Rev. Lett.* **1998**, *81*, 1203–1206. [CrossRef]
6. Chabé, J.; Lemarié, G.; Grémaud, B.; Delande, D.; Szriftgiser, P.; Garreau, J.C. Experimental Observation of the Anderson Metal-Insulator Transition with Atomic Matter Waves. *Phys. Rev. Lett.* **2008**, *101*, 255702. [CrossRef]
7. Lopez, M.; Clément, J.F.; Szriftgiser, P.; Garreau, J.C.; Delande, D. Experimental Test of Universality of the Anderson Transition. *Phys. Rev. Lett.* **2012**, *108*, 095701. [CrossRef]

8. Tian, C.; Altland, A. Field theory of Anderson transition of the kicked rotor. *Phys. Scr.* **2012**, *2012*, 014049. [CrossRef]
9. Sadgrove, M.; Wimberger, S.; Parkins, S.; Leonhardt, R. Ballistic and Localized Transport for the Atom Optics Kicked Rotor in the Limit of a Vanishing Kicking Period. *Phys. Rev. Lett.* **2005**, *94*, 174103. [CrossRef]
10. Ryu, C.; Andersen, M.F.; Vaziri, A.; d'Arcy, M.B.; Grossman, J.M.; Helmerson, K.; Phillips, W.D. High-Order Quantum Resonances Observed in a Periodically Kicked Bose-Einstein Condensate. *Phys. Rev. Lett.* **2006**, *96*, 160403. [CrossRef]
11. Kanem, J.F.; Maneshi, S.; Partlow, M.; Spanner, M.; Steinberg, A.M. Observation of High-Order Quantum Resonances in the Kicked Rotor. *Phys. Rev. Lett.* **2007**, *98*, 083004. [CrossRef] [PubMed]
12. Ammann, H.; Gray, R.; Shvarchuck, I.; Christensen, N. Quantum Delta-Kicked Rotor: Experimental Observation of Decoherence. *Phys. Rev. Lett.* **1998**, *80*, 4111–4115. [CrossRef]
13. d'Arcy, M.B.; Godun, R.M.; Oberthaler, M.K.; Cassettari, D.; Summy, G.S. Quantum Enhancement of Momentum Diffusion in the Delta-Kicked Rotor. *Phys. Rev. Lett.* **2001**, *87*, 074102. [CrossRef] [PubMed]
14. Sadgrove, M.; Hilliard, A.; Mullins, T.; Parkins, S.; Leonhardt, R. Observation of robust quantum resonance peaks in an atom optics kicked rotor with amplitude noise. *Phys. Rev. E* **2004**, *70*, 036217. [CrossRef] [PubMed]
15. Chai, S.; Fekete, J.; McDowall, P.; Coop, S.; Lindballe, T.; Andersen, M.F. Survival resonances in an atom-optics system driven by temporally and spatially periodic dissipation. *Phys. Rev. A* **2018**, *97*, 033616. [CrossRef]
16. Wu, S.; Tonyushkin, A.; Prentiss, M.G. Observation of Saturation of Fidelity Decay with an Atom Interferometer. *Phys. Rev. Lett.* **2009**, *103*, 034101. [CrossRef] [PubMed]
17. Talukdar, I.; Shrestha, R.; Summy, G.S. Sub-Fourier Characteristics of a δ-kicked-rotor Resonance. *Phys. Rev. Lett.* **2010**, *105*, 054103. [CrossRef] [PubMed]
18. Shrestha, R.K.; Wimberger, S.; Ni, J.; Lam, W.K.; Summy, G.S. Fidelity of the quantum δ-kicked accelerator. *Phys. Rev. E* **2013**, *87*, 020902. [CrossRef] [PubMed]
19. Duffy, G.J.; Parkins, S.; Müller, T.; Sadgrove, M.; Leonhardt, R.; Wilson, A.C. Experimental investigation of early-time diffusion in the quantum kicked rotor using a Bose-Einstein condensate. *Phys. Rev. E* **2004**, *70*, 056206. [CrossRef]
20. Behinaein, G.; Ramareddy, V.; Ahmadi, P.; Summy, G.S. Exploring the Phase Space of the Quantum δ-Kicked Accelerator. *Phys. Rev. Lett.* **2006**, *97*, 244101. [CrossRef] [PubMed]
21. White, D.H.; Ruddell, S.K.; Hoogerland, M.D. Experimental realization of a quantum ratchet through phase modulation. *Phys. Rev. A* **2013**, *88*, 063603. [CrossRef]
22. Sadgrove, M.; Horikoshi, M.; Sekimura, T.; Nakagawa, K. Rectified Momentum Transport for a Kicked Bose-Einstein Condensate. *Phys. Rev. Lett.* **2007**, *99*, 043002. [CrossRef] [PubMed]
23. Dana, I.; Ramareddy, V.; Talukdar, I.; Summy, G.S. Experimental Realization of Quantum-Resonance Ratchets at Arbitrary Quasimomenta. *Phys. Rev. Lett.* **2008**, *100*, 024103. [CrossRef] [PubMed]
24. Sadgrove, M.; Schell, T.; Nakagawa, K.; Wimberger, S. Engineering quantum correlations to enhance transport in cold atoms. *Phys. Rev. A* **2013**, *87*, 013631. [CrossRef]
25. Ni, J.; Dadras, S.; Lam, W.K.; Shrestha, R.K.; Sadgrove, M.; Wimberger, S.; Summy, G.S. Hamiltonian Ratchets with Ultra-Cold Atoms. *Annalen der Physik* **2017**, *529*, 1600335. [CrossRef]
26. Hainaut, C.; Rançon, A.; Clément, J.F.M.C.; Garreau, J.C.; Szriftgiser, P.; Chicireanu, R.; Delande, D. Ratchet effect in the quantum kicked rotor and its destruction by dynamical localization. *Phys. Rev. A* **2018**, *97*, 061601. [CrossRef]
27. Eltschka, C.; Schlagheck, P. Resonance- and Chaos-Assisted Tunneling in Mixed Regular-Chaotic Systems. *Phys. Rev. Lett.* **2005**, *94*, 014101. [CrossRef] [PubMed]
28. Shrestha, R.K.; Ni, J.; Lam, W.K.; Summy, G.S.; Wimberger, S. Dynamical tunneling of a Bose-Einstein condensate in periodically driven systems. *Phys. Rev. E* **2013**, *88*, 034901. [CrossRef]
29. Dadras, S.; Gresch, A.; Groiseau, C.; Wimberger, S.; Summy, G.S. Quantum Walk in Momentum Space with a Bose-Einstein Condensate. *Phys. Rev. Lett.* **2018**, *121*, 070402. [CrossRef]
30. Wang, J.; Gong, J. Proposal of a cold-atom realization of quantum maps with Hofstadter's butterfly spectrum. *Phys. Rev. A* **2008**, *77*, 031405. [CrossRef]
31. Ho, D.Y.H.; Gong, J. Quantized Adiabatic Transport In Momentum Space. *Phys. Rev. Lett.* **2012**, *109*, 010601. [CrossRef] [PubMed]

32. Wang, H.; Ho, D.Y.H.; Lawton, W.; Wang, J.; Gong, J. Kicked-Harper model versus on-resonance double-kicked rotor model: From spectral difference to topological equivalence. *Phys. Rev. E* **2013**, *88*, 052920. [CrossRef] [PubMed]
33. Chen, Y.; Tian, C. Planck's Quantum-Driven Integer Quantum Hall Effect in Chaos. *Phys. Rev. Lett.* **2014**, *113*, 216802. [CrossRef] [PubMed]
34. Dana, I. Topological properties of adiabatically varied Floquet systems. *Phys. Rev. E* **2017**, *96*, 022216. [CrossRef] [PubMed]
35. Zhou, L.; Gong, J. Floquet topological phases in a spin-1/2 double kicked rotor. *Phys. Rev. A* **2018**, *97*, 063603. [CrossRef]
36. Scharf, R. Kicked rotator for a spin-1/2 particle. *J. Phys. A: Math. Gen.* **1989**, *22*, 4223. [CrossRef]
37. Hernández, G.; Romanelli, A. Resonant quantum kicked rotor with two internal levels. *Phys. Rev. A* **2013**, *87*, 042316. [CrossRef]
38. Summy, G.; Wimberger, S. Quantum random walk of a Bose-Einstein condensate in momentum space. *Phys. Rev. A* **2016**, *93*, 023638. [CrossRef]
39. Kitagawa, T. Topological phenomena in quantum walks: elementary introduction to the physics of topological phases. *Quantum Inf. Process.* **2012**, *11*, 1107–1148. [CrossRef]
40. Sadgrove, M.; Wimberger, S.; Parkins, S.; Leonhardt, R. Scaling law and stability for a noisy quantum system. *Phys. Rev. E* **2008**, *78*, 025206. [CrossRef]
41. Izrailev, F.M. Simple models of quantum chaos: Spectrum and eigenfunctions. *Phys. Rep.* **1990**, *196*, 299–392. [CrossRef]
42. Groiseau, C.; Gresch, A.; Wimberger, S. Quantum walks of kicked Bose? Einstein condensates. *J. Phys. A: Math. Theor.* **2018**, *51*, 275301. [CrossRef]
43. Wimberger, S. *Nonlinear Dynamics and Quantum Chaos: An Introduction*; Graduate Texts in Physics; Springer International Publishing: Cham, Switzerland, 2014.
44. Press, W.H.; Teukolsky, S.A.; Vetterling, W.T.; Flannery, B.P. *Numerical Recipes in C++*; Cambridge University Press: Cambridge, UK, 2002.
45. Weiß, M.; Groiseau, C.; Lam, W.K.; Burioni, R.; Vezzani, A.; Summy, G.S.; Wimberger, S. Steering random walks with kicked ultracold atoms. *Phys. Rev. A* **2015**, *92*, 033606. [CrossRef]
46. Asbóth, J.K. Symmetries, topological phases, and bound states in the one-dimensional quantum walk. *Phys. Rev. B* **2012**, *86*, 195414. [CrossRef]
47. Ho, D.Y.H.; Gong, J. Topological effects in chiral symmetric driven systems. *Phys. Rev. B* **2014**, *90*, 195419. [CrossRef]
48. Cayssol, J.; Dora, B.; Simon, F.; Moessner, R. Floquet topological insulators. *Phys. Status Solidi (RRL)* **2013**, *7*, 101–108. [CrossRef]